Applications of the modified Rydberg antiblockade regime with simultaneous driving

Shi-Lei Su,[1,*] Yongzhi Tian,[1] H. Z. Shen,[2,†] Huaping Zang,[1,‡] Erjun Liang,[1] and Shou Zhang[3,4]

[1]*School of Physical Science & Engineering and Key Laboratory of Materials Physics of Ministry of Education of China, Zhengzhou University, Zhengzhou 450052, People's Republic of China*

[2]*Center for Quantum Sciences and School of Physics, Northeast Normal University, Changchun 130024, People's Republic of China*

[3]*Department of Physics, College of Science, Yanbian University, Yanji, Jilin 133002, People's Republic of China*

[4]*Department of Physics, Harbin Institute of Technology, Harbin 150001, People's Republic of China*

(Received 7 August 2017; published 25 October 2017)

Through analyzing the effective dynamics of two Rydberg atoms under the dispersive coupling process, we give a method to modify the traditional antiblockade regime with simultaneous driving without adding any extra controls and resources. The modified regime can be used to construct controlled-PHASE and controlled-NOT gates in one step without manipulating the shape and amplitude, and tailoring sequences of the driving pulses. For the controlled-PHASE gate, only one pumping process from the ground state to the Rydberg state of each atom is required thus the resource is minimal. And the atomic addressability is not necessary. The scheme can be improved a lot after adding single-qubit operations since arbitrary phases can be achieved accurately with a short period of evolution time. For one-step construction of controlled-NOT gate, two schemes with high fidelities are given and discussed. Besides, the modified regime can also be used to improve the performance of the dissipation-based quantum entanglement preparation scheme. The optimal value of the modified condition for entanglement preparation is discussed for a wide range of parameters. Our study enriches the physics and applications of the simultaneous-driving-based Rydberg antiblockade regime without adding any operation complexity.

DOI: 10.1103/PhysRevA.96.042335

I. INTRODUCTION

The classical laser field with resonant frequency driving a ground state to the Rydberg state of one atom cannot excite two or more Rydberg atoms simultaneously [1,2]; this interesting phenomenon is called the Rydberg blockade. The root cause for this phenomenon is that the collective jumped Rydberg states would interact directly and strongly with each other within the blockade radius range due to their large electric dipole [3–5]. Based on the Rydberg blockade regime, the conditional dynamics can be easily constructed through driving the atoms step by step [1,2,6–10]. The phase [1] or the exchange between two ground states of the latter Rydberg atoms [7] based on electromagnetically induced transparency would be achieved or not conditioned on whether the former atom is excited to the Rydberg state. Besides, combining adiabatic passage and the Rydberg blockade regime can also lead to robust creation of the maximal entanglement and quantum logic gates [11–18]. Experimentally, a suppression of the excitation in the Rydberg gas [19–21] and the evidence for coherent Rydberg excitation of frozen Rydberg gases in the strong blockade regime [22] have been observed. And the blockade with two Rydberg atoms [23,24] have been demonstrated. Recently, entanglement between neutral atoms [25], optical nonlinearity [26], many-body quantum dynamics [27–29], and the energy transport [30] induced by the Rydberg blockade have also been observed.

The Rydberg blockade can be generalized to Rydberg atoms that largely stay in the ground state via the Rydberg-dressed state method [31–39], whereby dispersive Rydberg excitation admixes a small percentage of the Rydberg state into the ground-state wave function. Via the Rydberg-dressed state method, many-body interferometry of the spin lattice [40] and the entanglement with the spin-flip blockade [41] are realized experimentally. Besides, the Rydberg interactions and the induced blockade phenomenon are also useful for achievement of the quantum devices, such as the single-photon switch [42], quantum filter [43], single-photon transistor [44,45], etc. In addition, the photon-photon interactions can be generated via the Rydberg blockade [46,47]. And the blockade of the photon is also interesting [48].

In stark contrast to the blockade regime, Ates *et al.* [49] predicted a Rydberg antiblockade (RAB) regime in a three-level scheme when interaction energy matches the Rabi frequency of the lower transition in an ultracold lattice gas. Amthor *et al.* demonstrated [50] in the antiblockade regime in experiment even the atomic interaction shift is much greater than the excitation line width when the system is initially set as an unstructured gas. Despite the fact that the population of the two-atom Rydberg excited state is not higher than 0.2 [49,50], these schemes pave the way for the RAB regime. Besides, Pohl *et al.* showed that the RAB regime would emerge for three Rydberg atoms if the dark state of the whole system that contained three excited Rydberg atoms was populated [51]. Immediately, the antiblockade between two Rydberg atoms was studied when the atoms were illuminated by a zero-area phase-jump pulse [52].

The critical condition to achieve the simultaneous-driving-based RAB regime was given by Zuo *et al.* [53] and Lee *et al.* [54]. The main starting point is to compensate the energy shift induced by the Rydberg-Rydberg interaction by modulating the detuning between the driving field and atomic transition. The application and advantage of this RAB regime become apparent when the dissipative processes are considered by Carr and Saffman [55] for preparation of entanglement. However,

*slsu@zzu.edu.cn
†shenhz458@nenu.edu.cn
‡zanghuaping@sina.com

constructing the quantum logic operations based on the traditional RAB regime [53,54] is challenging since some extra unwanted Stark shift terms would emerge inevitably in the effective Hamiltonian of the traditional RAB-based scheme when two ground states of each Rydberg atom are involved and the large detuning condition is satisfied.

The above studies for the RAB regime refers specially to the simultaneous-driving-based case. The merit is that the regime can be realized in one step [53,54] and can be further used to prepare entanglement via the aid of dissipative dynamics [55,56] or not [53]. Besides, in Ref. [57], the authors propose a completely different RAB regime with sequent driving which pumps the Rydberg atoms one by one. Each of the two kinds of antiblockade regimes is able to realize the collective excitation of Rydberg atoms and find corresponding applications in quantum information processing (QIP). The differences between the simultaneous-driving-based (the former) and the sequent-driving-based (the latter) RAB regimes can be summarized as follows. (i) The former regime is based on the second-order perturbation theory while the latter regime is based on the accurate excitation process without approximation. (ii) The former regime can be realized in one step while the latter one can be realized fast. (iii) The former regime does not require atom addressability, which is not the case of the latter one. (iv) The former regime is convenient for preparing entanglement while the latter one is feasible for construction of the quantum logic gate.

In this paper, we modify the traditional RAB regime [53–55] with simultaneous driving by compensating not only the energy shift induced by the Rydberg-Rydberg interaction, but also the energy associated with some of the Stark shift induced by the dispersive interactions without adding extra lasers and controls. We show that, in contrast to the traditional RAB regime with simultaneous driving,one the modified one (i) can be utilized to construct the controlled-PHASE gate, and (ii) can be used to construct the controlled-NOT gate. Different from the blockade-based schemes, our scheme can construct the quantum controlled-PHASE gate in one-step approximately or two-step accurately (with arbitrary conditional phases) through adding single-qubit operations without adiabatic controls. Besides, the modified regime is able to be used to construct the quantum controlled-NOT gate directly in one step without adiabatic controls. In addition, the modified RAB (iii) can also improve the efficiency of the dissipative dynamics-based schemes for entanglement generation. Our study enriches the physics and applications of the simultaneous-driving-based RAB regime.

II. BASIC MODEL AND THE MODIFIED RAB REGIME

A. Basic model

As shown in Fig. 1(a), we consider two Rydberg atoms trapped in optical tweezers. Each of the atoms has two ground states, and one of the ground states $|1\rangle$ is coupled to the Rydberg state $|r\rangle$ via the two-photon process shown in Fig. 1(b) or single-photon transition shown in Fig. 1(c). If the condition $\delta \gg \{\Omega_1/2, \Omega_2/2\}$ is satisfied, one can adiabatically eliminate the intermediate energy level $|p\rangle$. The model in Fig. 1(b) would be equivalent to that in Fig. 1(c) with $\Delta_1 - (\Omega_2)^2/(4\delta) = \Delta$

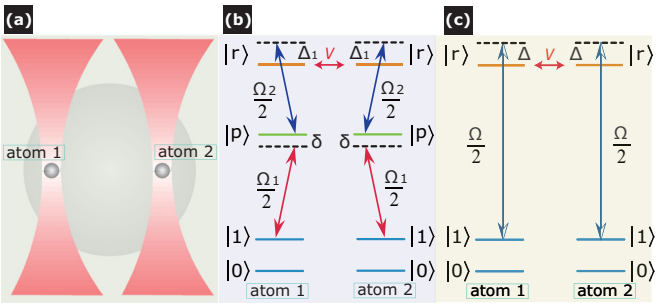

FIG. 1. (a) Schematic representation of two trapped Rydberg atoms. (b) Diagram of two four-energy-level Rydberg atoms. Each atom has two ground states $|0\rangle$ and $|1\rangle$, one short-lived state $|p\rangle$ and one Rydberg state $|r\rangle$. The ground state $|1\rangle$ is coupled to the Rydberg level $|r\rangle$ by a two-photon process via the intermediate energy level $|p\rangle$. The corresponding Rabi frequencies of the transition $|1\rangle \rightarrow |p\rangle$ and $|p\rangle \rightarrow |r\rangle$ are Ω_1 and Ω_2, respectively. (c) Diagram of two three-energy-level Rydberg atoms. Each atom has two ground states $|0\rangle$ and $|1\rangle$, and one Rydberg state $|r\rangle$. The transition from ground state $|1\rangle$ to $|r\rangle$ is coupled directly by a laser with Rabi frequency Ω. Experimentally, in Ref. [41], researchers used a 319-nm laser to couple the ^{133}Cs atom directly from the ground state to the Rydberg state, in a single-photon transition [58].

and $\Omega_1\Omega_2/(2\delta) = \Omega$, and canceling some Stark shift of energy level $|1\rangle$ through adding extra lasers. On the other hand, the model in Fig. 1(c) can be achieved in experiment directly [41,58] through encoding $|1\rangle \equiv |6S_{1/2}, F = 4, m_F = 0\rangle$, $|0\rangle \equiv |6S_{1/2}, F = 3, m_F = 0\rangle$, and $|r\rangle \equiv |84P_{3/2}; m_J\rangle$, and considering the exciting laser at $\lambda = 319$ nm. In the following, we only consider the model in Fig. 1(c) for simplicity.

In the rotation frame, the Hamiltonian of the system can be written as

$$\hat{H} = \hat{H}_1 + \hat{H}_2 + \hat{\mathscr{U}}, \tag{1}$$

where

$$\hat{H}_j = -\Delta|r\rangle_j\langle r| + \frac{\Omega}{2}(|r\rangle_j\langle 1| + \text{H.c.}), \tag{2}$$

and

$$\hat{\mathscr{U}} = V|rr\rangle\langle rr|. \tag{3}$$

With the dispersive regime condition $\Delta \gg \Omega/2$ and the traditional RAB condition $\Delta = V/2$ [53–55,59,60] being satisfied, the effective Hamiltonian of the whole system in the two-atom basis would be

$$\hat{H}_{\text{eff}} = \frac{\Omega^2}{4\Delta}[2(|11\rangle + |rr\rangle)(\langle 11| + \langle rr|) + (|10\rangle\langle 10| + |01\rangle\langle 01|)], \tag{4}$$

in which the second-order perturbation method is considered [61] and we have discarded the single excitation terms since they are in a closed subspace and not included in the initial states.

The Stark shift in Eq. (4) is the reason why the quantum logic gate cannot be implemented efficiently [62]. Besides, for the case of the dissipative-dynamics-based quantum entanglement preparation scheme, the Stark shift of $|rr\rangle\langle rr|$ may stretch the time of the system to be steady. If one can

modify the RAB regime to cancel some of the undesirable Stark-shift terms, the following relevant QIP schemes would be interesting.

B. Modified Rydberg antiblockade regime with simultaneous driving

We notice that the term relevant to the Rydberg-Rydberg interaction is $|rr\rangle\langle rr|$, and interestingly, one of the Stark-shift terms of the effective Hamiltonian (4) also has the same form. This inspires us to see whether we can modify V and Δ to cancel some of the unwanted Stark shift, and furthermore to achieve some useful QIP tasks. We first modify the RAB condition as [63]

$$V = 2\Delta - \mu\frac{\Omega^2}{2\Delta}\ [\mu \in \text{Reals}]. \tag{5}$$

When $\mu = 0$ is satisfied, Eq. (5) turns back to the traditional RAB condition with simultaneous driving. Otherwise, when $\mu \neq 0$ the effective Hamiltonian of Eq. (1) would be changed to [61] (see appendix)

$$\hat{H}_{\text{eff}} = \frac{\Omega^2}{4\Delta}[2(|11\rangle\langle 11| + |rr\rangle\langle 11| + |11\rangle\langle rr|) + 2(1-\mu)|rr\rangle\langle rr| + (|10\rangle\langle 10| + |01\rangle\langle 01|)]. \tag{6}$$

The value of μ is not constant, one can specify different values of μ for different QIP tasks. In fact, one would find that, even for a specific QIP task, there may be many options for the values of μ. These features enrich the physics and applications of the RAB regime with simultaneous driving. In the following, we illustrate how to choose μ to effectively achieve the quantum controlled-PHASE gate and -NOT gate, and improve the performance of the dissipative-dynamics-based quantum entanglement preparation scheme. Another thing that should be noted is that the introduction of μ can be realized through changing the Rabi frequency or detunings of the driving process. That is, the extra lasers or controls are not required on the basis of the traditional simultaneous-driving-based RAB regime.

III. QUANTUM LOGIC GATE

A. Quantum controlled-PHASE gate

The evolution operator related to Eq. (6), $e^{-i\hat{H}_{\text{eff}}t}$, induces

$$\begin{aligned}&|00\rangle \to |00\rangle, |01\rangle \to e^{-iv}|01\rangle, |10\rangle \to e^{-iv}|10\rangle,\\ &|11\rangle \to \frac{e^{i\mu_1 v}}{\mu_2}\{[\mu_2\cos(\mu_2 v) - i\mu\sin(\mu_2 v)]|11\rangle - 2i\sin(\mu_2 v)|rr\rangle\},\end{aligned} \tag{7}$$

in which $v = \Omega^2 t/(4\Delta)$, $\mu_1 = \mu - 2$, and $\mu_2 = \sqrt{\mu^2+4}$. The form of the controlled-PHASE gate is

$$\hat{U} = |00\rangle\langle 00| + |01\rangle\langle 01| + |10\rangle\langle 10| + e^{i\theta}|11\rangle\langle 11|. \tag{8}$$

The following analysis is based on Eq. (7), whose aim is to construct the quantum logic gate in Eq. (8).

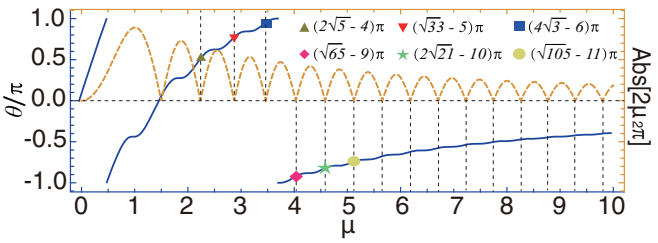

FIG. 2. Phase of $|11\rangle$ and the absolute value of the amplitude of $|rr\rangle$ versus μ, respectively, at the time $t = 8\pi\Delta/\Omega^2$. The conditional phase is accurate only when the amplitude of $|rr\rangle$ equals zero.

1. Approximate, one-step case

To construct the controlled-PHASE gate in one step, $|11\rangle$ should get a phase θ while the other states keep invariant. Therefore, $v = 2n\pi (n \in \text{Integer}$, we first consider $n = 1)$ should be satisfied in Eq. (7). And the coefficient of $|rr\rangle$ should be zero since it is out of the computational subspace. Consequently, μ_2 should be integral or half integral. Then the controlled-PHASE gate with the conditional phase $[2\mu\pi \text{ Mod } 2\pi]$(when μ_2 is integral) or $[(2\mu-1)\pi \text{ Mod } 2\pi]$ (when μ_2 is half integral) is constructed.

The phase θ of state $|11\rangle$ versus μ is shown in Fig. 2, from which one can find that although the results are analytical, the phase π and $\pi/2$ cannot be achieved. That is, the practicability of the gate would be discounted in the QIP tasks. In the following, we pay attention to construct controlled-$\pi/2$ and controlled-π gates approximately [64], in one step by choosing appropriate μ.

In Fig. 3(a), we plot the imaginary part of the coefficient of $|11\rangle$ versus μ with the precondition $t = 8\pi\Delta/\Omega^2$ being satisfied. One can see that the conditional phase $\theta = \pm\pi/2$

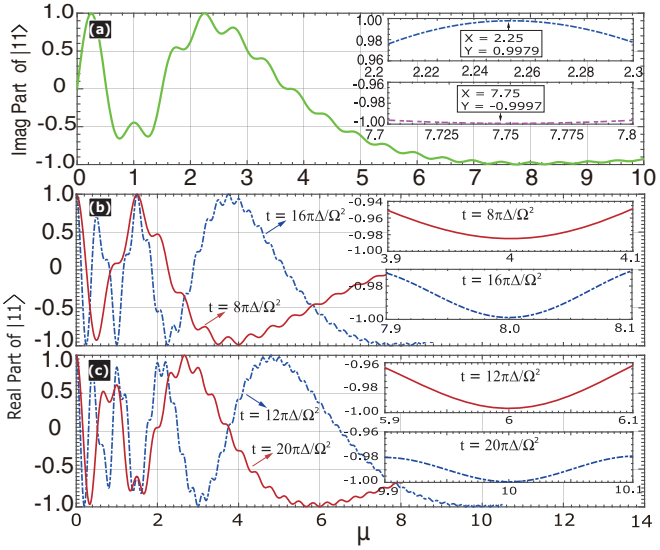

FIG. 3. (a) Imaginary part of the coefficient of $|11\rangle$ versus μ with the precondition $t = 8\pi\Delta/\Omega^2$ that keeps $|01\rangle$ and $|10\rangle$ invariant being satisfied. (b) and (c) Real part of the coefficient of $|11\rangle$ versus μ with (b) the precondition $t = 8\pi\Delta/\Omega^2$ or $t = 16\pi\Delta/\Omega^2$ and (c) the precondition $t = 12\pi\Delta/\Omega^2$ or $t = 20\pi\Delta/\Omega^2$ being satisfied, respectively.

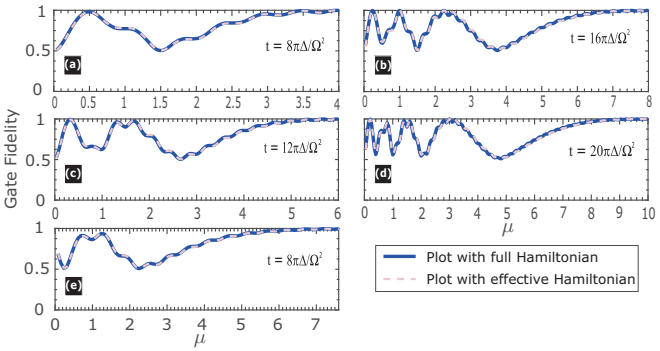

FIG. 4. Gate fidelity versus μ at different evolution times with $\Delta = 20\Omega$. The initial state is supposed as $|\psi_0\rangle = (|00\rangle + |01\rangle + |10\rangle + |11\rangle)/2$. The fidelity is plotted via Eqs. (9) and (10). (a) and (b) Fidelity of the standard controlled-π gate. (c) and (d) Fidelity of the gate $\hat{U} = |00\rangle\langle 00| - |01\rangle\langle 01| - |10\rangle\langle 10| - |11\rangle\langle 11|$. (e) Fidelity of the gate $\hat{U} = |00\rangle\langle 00| + |01\rangle\langle 01| + |10\rangle\langle 10| + e^{-i\pi/2}|11\rangle\langle 11|$.

can be approximately achieved when μ equals 2.25 and 7.75, respectively.

In Figs. 3(b) and 3(c), we plot the real part of $|11\rangle$ versus μ with the preconditions $t = 8\pi\Delta/\Omega^2$ and $16\pi\Delta/\Omega^2$, $12\pi\Delta/\Omega^2$ and $20\pi\Delta/\Omega^2$ being fulfilled, respectively. From the numerical results in Fig. 3(b), one can find that if $\mu = 4$, the transformation $|11\rangle \to -0.985|11\rangle$ would be achieved and the other three computation bases keep invariant at the time $t = 8\pi\Delta/\Omega^2$. Besides, if $\mu = 8$ is satisfied, the conditional phase $|11\rangle \to -0.999|11\rangle$ would be achieved at the time $t = 16\pi\Delta/\Omega^2$. That is, the controlled-π gate is constructed.

One should note $\mu = 7.75$ is also feasible for realization of the controlled-π gate [65]. In Fig. 3(c), we plot the real part of $|11\rangle$ versus μ with the preconditions $t = 12\pi\Delta/\Omega^2$ and $20\pi\Delta/\Omega^2$ being fulfilled, respectively. At these two evolution times, the transformations $|01(10)\rangle \to -|01(10)\rangle$ are realized. Then, if one chooses μ to achieve $|11\rangle \to -|11\rangle$, the operations $\hat{U} = |00\rangle\langle 00| - |01\rangle\langle 01| - |10\rangle\langle 10| - |11\rangle\langle 11|$ would be constructed, which is equivalent to the controlled-π gate through adding single-qubit operations. And we call this controlled-π' gate in the following. From Fig. 3(c), one can get for the case $t = 12\pi\Delta/\Omega^2$, $|11\rangle \to -0.997|11\rangle$ is achieved when $\mu = 6$. For the case $t = 20\pi\Delta/\Omega^2$, $|11\rangle \to -0.999|11\rangle$ is achieved when $\mu = 10$.

A measure of the distance between two quantum states is the fidelity [66],

$$F = \mathrm{tr}\sqrt{\hat{\rho}^{1/2}\hat{\sigma}\,\hat{\rho}^{1/2}}. \tag{9}$$

For a specific input state, one can use the fidelity between the output state ($\hat{\sigma}$) generated by the ideal quantum logic gate and that ($\hat{\rho}$) generated by the practical logic gate to access the performance of the scheme. The following Schrödinger equation,

$$\dot{\hat{\rho}}(t) = -i[\hat{H}, \hat{\rho}(t)], \tag{10}$$

is used to get the final state of the scheme.

In Fig. 4, one can see that (i) the curves plotted by full and effective Hamiltonians agree well with each other, which proves the validity of the effective Hamiltonian. And (ii) the gate fidelity is close to unity when μ takes the optimal value

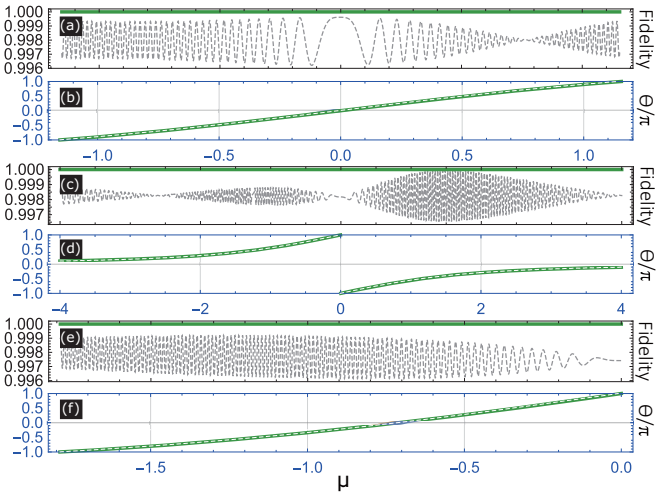

FIG. 5. (a), (c), and (f) Gate fidelity plotted versus μ under effective (solid line) and full (dashed line) Hamiltonians with $\mu_2\nu = 2\pi(\pi, 3\pi)$ and $\Delta = 12\Omega$. The initial state is set as $(|00\rangle + |01\rangle + |10\rangle + |11\rangle)/2$. (b), (d), and (f) Conditional phase plotted by effective (solid line) and full (dashed line) Hamiltonians versus μ with $\mu_2\nu = 2\pi(\pi, 3\pi)$ and $\Delta = 12\Omega$.

predicted by Fig. 3. Besides, each point with high fidelity in Fig. 4 has its corresponding point predicated by the displayed curves in Fig. 3.

2. *Accurate, analytical, arbitrary phase, two-step case*

Suppose the parameters in Eq. (7) satisfy $\mu_2\nu = 2n\pi$ or $(2n+1)\pi$ at a given time, $|11\rangle$ would get an accurate phase $\theta' = \mu_1\nu$ or $\pi + \mu_1\nu$ accordingly. At the same time, $|01\rangle$ and $|10\rangle$ would both get a phase $\varphi = -\nu$. Then if one performs a single-qubit operation on $|1\rangle$ to eliminate the phases of $|01\rangle$ and $|10\rangle$, the phase of $|11\rangle$ would be changed to $\theta = \theta' - 2\varphi = \mu\nu$ for $\mu_2\nu = 2n\pi$ and to $\pi + \mu\nu$ for $\mu_2\nu = (2n+1)\pi$, respectively.

We first consider the case $\mu_2\nu = 2\pi$, i.e., $\nu = 2\pi/\mu_2$. Then $\theta = \mu\nu \equiv 2\pi\mu/\sqrt{\mu^2+4}$ is achieved. One can easily get that $\theta = \pm\pi$ when $\mu = \pm\sqrt{4/3}$, and θ is monotonically for $\mu \in [-\sqrt{4/3}, \sqrt{4/3}]$. In other words, the arbitrary conditional phase from $-\pi$ to π can be achieved analytically with appropriate μ, as shown in Fig. 5(b).

For the case $\mu_2\nu = \pi$, $\theta = \pi + \mu\nu \equiv \pi + \mu\pi/\sqrt{\mu^2+4}$. One cannot find an appropriate μ to realize $\theta = 0$. That is, the phase with the arbitrary angle is a challenge for $\mu_2\nu = \pi$. Nevertheless, $\theta \in [\pi - 2\pi/\sqrt{5}, \pi]$ and $[-\pi, 2\pi/\sqrt{5} - \pi]$, which include $\pm\pi/8$, $\pm\pi/4$, $\pm\pi/2$, and $\pm\pi$, are achievable for $\mu \in [-4, 4]$, respectively, as shown in Fig. 5(d).

For the case $\mu_2\nu = 3\pi$, $\theta = \pi + \mu\nu \equiv \pi + 3\mu\pi/\sqrt{\mu^2+4}$. One can find that $\theta = \pi$ or $-\pi$ when $\mu = 0$ or $(-\sqrt{16/5})$, and θ is monotonically for $\mu \in [-\sqrt{16/5}, 0]$. In other words, the conditional phase with the arbitrary angle is achievable, as shown in Fig. 5(f).

Besides, we plot the conditional phase under the full Hamiltonian with $\Delta = 12\Omega$ for $\mu_2\nu = 2\pi(\pi, 3\pi)$ in Figs. 5(b), 5(d) and 5(f) (dashed line). In addition, the gate fidelities under the effective and full Hamiltonian with one group of specific

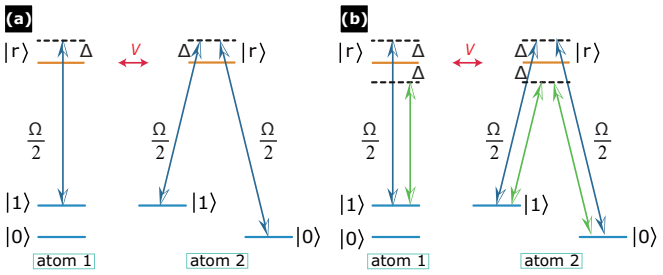

FIG. 6. Energy diagram for one-step implementation of controlled-NOT gate between two Rydberg atoms. (a) Constructing the controlled-NOT gate approximately with economic resources. (b) Analytical model to construct the controlled-NOT gate through adding one laser field on control atom and one Raman process on target atom, respectively.

initial states are also plotted in Figs. 5(a), 5(c) and 5(e). These studies show the analysis of the two-step scheme is feasible.

In contrast to the one-step case, these two-step schemes are analytical and can be implemented accurately with a shorter evolution time. Besides, the arbitrary conditional phase is achievable through adjusting μ correspondingly.

B. Quantum controlled-NOT gate

In this subsection, we focus on the quantum controlled-NOT gate via the modified RAB regime. As shown in Fig. 6(a), we first consider the system with the Hamiltonian,

$$\hat{H} = \hat{H}_1 + \hat{H}_2 + \hat{\mathscr{U}}, \tag{11}$$

where

$$\hat{H}_1 = -\Delta|r\rangle_1\langle r| + \frac{\Omega}{2}(|r\rangle_1\langle 1| + \text{H.c.}),$$
$$\hat{H}_2 = -\Delta|r\rangle_2\langle r| + \frac{\Omega}{2}(|r\rangle_2\langle 1| + |r\rangle_2\langle 0| + \text{H.c.}), \tag{12}$$

and

$$\hat{\mathscr{U}} = V|rr\rangle\langle rr|. \tag{13}$$

Then, under the traditional RAB regime $V = 2\Delta$ and dispersive regime condition $\Delta \gg \Omega/2$, the effective form of the Hamiltonian (11) would be

$$\hat{H}_{\text{eff}} = \frac{\Omega^2}{2\Delta}[(|10\rangle + |11\rangle)\langle rr| + \text{H.c.}] + \frac{3\Omega^2}{4\Delta}|rr\rangle\langle rr| + \frac{\Omega^2}{4\Delta}(2|10\rangle\langle 10| + 2|11\rangle\langle 11| + |01\rangle\langle 01| + |00\rangle\langle 00|) + \frac{\Omega^2}{4\Delta}(|00\rangle\langle 01| + |10\rangle\langle 11| + \text{H.c.}), \tag{14}$$

in which we have ignored the terms in the single excitation subspace since they are not included in the initial states and also do not interact with other states. The form of the controlled-NOT gate is

$$\hat{U} = |00\rangle\langle 00| + |01\rangle\langle 01| + |11\rangle\langle 10| + |10\rangle\langle 11|. \tag{15}$$

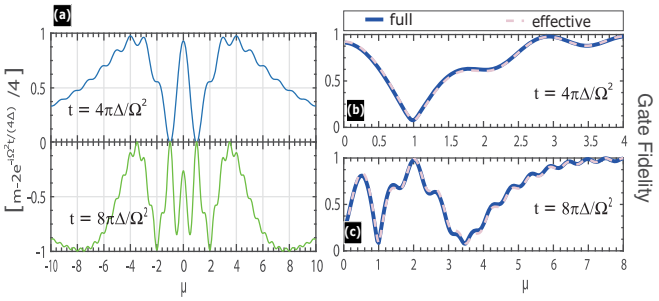

FIG. 7. (a) Values of the real part of $[m - 2e^{-i\Omega^2 t/(4\Delta)}]/4$ versus μ at two different evolution times. (b) and (c) Gate fidelity versus μ with the condition $\Delta = 20\Omega$ for two different evolution times with the specific initial state $|\psi_0\rangle = (0.1|00\rangle + 0.1|01\rangle + |10\rangle + 0.05|11\rangle)/N$ (N is the normalization coefficient). The fidelity is plotted via Eqs. (9) and (10). (b) Fidelity of the standard controlled-NOT gate. (c) Fidelity of the controlled-NOT′ gate $\hat{U} = |00\rangle\langle 00| + |01\rangle\langle 01| - |11\rangle\langle 10| - |10\rangle\langle 11|$.

1. Approximate case

Under the modified RAB condition in Eq. (5), the effective Hamiltonian can be modified to

$$\hat{H}_{\text{eff}} = \frac{\Omega^2}{2\Delta}[(|10\rangle + |11\rangle)\langle rr| + \text{H.c.}] + \frac{\Omega^2}{4\Delta}(3 - 2\mu)|rr\rangle\langle rr| + \frac{\Omega^2}{4\Delta}(2|10\rangle\langle 10| + 2|11\rangle\langle 11| + |01\rangle\langle 01| + |00\rangle\langle 00|) + \frac{\Omega^2}{4\Delta}(|00\rangle\langle 01| + |10\rangle\langle 11| + \text{H.c.}). \tag{16}$$

The evolution process dominated by Eq. (16) is

$$\begin{aligned}
|00\rangle &\to \frac{1}{2}\left[\left(1 + e^{\frac{-i\Omega^2 t}{2\Delta}}\right)|00\rangle + \left(-1 + e^{\frac{-i\Omega^2 t}{2\Delta}}\right)|01\rangle\right],\\
|01\rangle &\to \frac{1}{2}\left[\left(-1 + e^{\frac{-i\Omega^2 t}{2\Delta}}\right)|00\rangle + \left(1 + e^{\frac{-i\Omega^2 t}{2\Delta}}\right)|01\rangle\right],\\
|10\rangle &\to \frac{1}{4}\left[\left(m + 2e^{\frac{-i\Omega^2 t}{4\Delta}}\right)|10\rangle + \left(m - 2e^{\frac{-i\Omega^2 t}{4\Delta}}\right)|11\rangle\right]\\
&\quad - \frac{1}{\mu_5}e^{\frac{-i\mu_4\Omega^2 t}{4\Delta}}\left(e^{\frac{i\mu_5\Omega^2 t}{2\Delta}} - 1\right)|rr\rangle,\\
|11\rangle &\to \frac{1}{4}\left[\left(m - 2e^{\frac{-i\Omega^2 t}{4\Delta}}\right)|10\rangle + \left(m + 2e^{\frac{-i\Omega^2 t}{4\Delta}}\right)|11\rangle\right]\\
&\quad - \frac{1}{\mu_5}e^{\frac{-i\mu_4\Omega^2 t}{4\Delta}}\left(e^{\frac{i\mu_5\Omega^2 t}{2\Delta}} - 1\right)|rr\rangle,
\end{aligned} \tag{17}$$

in which $\mu_3 = -3 + \mu + \sqrt{8 + \mu^2}$, $\mu_4 = 3 - \mu + \sqrt{8 + \mu^2}$, $\mu_5 = \sqrt{8 + \mu^2}$, and $m = e^{i\mu_3\Omega^2 t/(4\Delta)}(1 - \mu/\mu_5) + e^{-i\mu_4\Omega^2 t/(4\Delta)}(1 + \mu/\mu_5)$. Therefore, if one can choose the evolution time and parameters to make $[1 + e^{-i\Omega^2 t/(2\Delta)}]/2 = 1$ and $[m - 2e^{i\Omega^2 t/(4\Delta)}]/4 = 1$ being satisfied simultaneously, the desired quantum logic gate is achieved. The first condition can be easily satisfied if one chooses the condition $\Omega^2 t/(2\Delta) = 2n\pi$ ($n \in$ Integer). The second condition cannot be satisfied for $\mu = 0$, which corresponds to the traditional RAB regime.

In Fig. 7(a), we plot the real part of $[m - 2e^{-i\Omega^2 t/(4\Delta)}]/4$ to find suitable μ. It is obvious that, when $t = 4\pi\Delta/\Omega^2$ and $\mu = \pm 4$ are satisfied, the real part of $[m - 2e^{-i\Omega^2 t/(4\Delta)}]/4$ is close to

1 and the desired logic operation in Eq. (15) would be achieved approximately. Besides, when $t = 8\pi\Delta/\Omega^2$ and $\mu = \pm 2, \pm 7.5, \pm 8$ are satisfied, the real part of $[m - 2e^{-i\Omega^2 t/(4\Delta)}]/4$ is close to -1 and the logic gate $\hat{U} = |00\rangle\langle 00| + |01\rangle\langle 01| - |11\rangle\langle 10| - |10\rangle\langle 11|$(we call it controlled-NOT′ gate), which is equivalent to the standard controlled-NOT gate through adding one single-qubit operation, can be constructed. In Figs. 7(b) and 7(c), we plot the fidelity of the controlled-NOT gate with one specific initial state. One can see that the curves plotted by effective and full Hamiltonians agree well with each other, and the fidelity approaches to unity around the values of μ given by the former analysis.

2. Accurate cases

Through adding one laser filed on the control atom and one Raman process on the target atom, respectively, as shown in Fig. 6(b), $\hat{H}_1$ and $\hat{H}_2$ is changed to

$$\hat{H}_1 = -\Delta|r\rangle_1\langle r| + \frac{\Omega}{2}(|r\rangle_1\langle 1| + |r\rangle_1\langle 1|e^{2i\Delta t} + \text{H.c.}),$$
$$\hat{H}_2 = -\Delta|r\rangle_2\langle r| + \frac{\Omega}{2}(|r\rangle_2\langle 1| + |r\rangle_2\langle 0| + \text{H.c.}) + \frac{\Omega}{2}(|r\rangle_2\langle 1|e^{2i\Delta t} + |r\rangle_2\langle 0|e^{2i\Delta t} + \text{H.c.}), \quad (18)$$

and the rest of the system Hamiltonian is the same as that of the model described in Fig. 6(a). Under the modified RAB regime and dispersive regime condition $\Delta \gg \Omega/2$, the effective Hamiltonian would be

$$\hat{H}_{\text{eff}} = \frac{\Omega^2}{2\Delta}\{[(|10\rangle + |11\rangle)\langle rr| + \text{H.c.}] + (2-\mu)|rr\rangle\langle rr|\}. \quad (19)$$

If $\mu = 2$, the Hamiltonian would be further simplified to

$$\hat{H}_{\text{eff}} = \frac{\Omega^2}{2\Delta}[(|10\rangle + |11\rangle)\langle rr| + \text{H.c.}], \quad (20)$$

which induces the following evolution processes:

$$|00\rangle \to |00\rangle, |01\rangle \to |01\rangle,$$
$$|10\rangle \to \left[\cos\left(\frac{\Omega^2 t}{2\sqrt{2}\Delta}\right)\right]^2|10\rangle - \left[\sin\left(\frac{\Omega^2 t}{2\sqrt{2}\Delta}\right)\right]^2|11\rangle - \frac{i}{\sqrt{2}}\sin\left(\frac{\Omega^2 t}{\sqrt{2}\Delta}\right)|rr\rangle,$$
$$|11\rangle \to -\left[\sin\left(\frac{\Omega^2 t}{2\sqrt{2}\Delta}\right)\right]^2|10\rangle + \left[\cos\left(\frac{\Omega^2 t}{2\sqrt{2}\Delta}\right)\right]^2|11\rangle - \frac{i}{\sqrt{2}}\sin\left(\frac{\Omega^2 t}{\sqrt{2}\Delta}\right)|rr\rangle. \quad (21)$$

If $t = \sqrt{2}\pi\Delta/\Omega^2$ is fulfilled, the controlled-NOT′ gate is achieved.

Besides, if one modifies the relative phase of the Rabi frequencies to change $\hat{H}_2$ as

$$\hat{H}_2 = -\Delta|r\rangle_2\langle r| + \frac{\Omega}{2}(|r\rangle_2\langle 1| - |r\rangle_2\langle 0| + \text{H.c.}) + \frac{\Omega}{2}(|r\rangle_2\langle 1|e^{2i\Delta t} - |r\rangle_2\langle 0|e^{2i\Delta t} + \text{H.c.}), \quad (22)$$

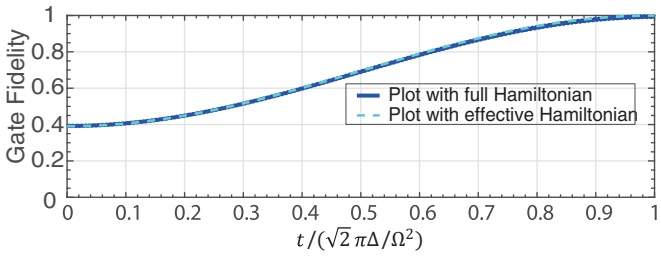

FIG. 8. Fidelity of the standard controlled-NOT gate versus evolution time. The initial state is chosen as $|\psi_0\rangle = (0.2|00\rangle + 0.2|01\rangle + 0.5|10\rangle + 0.05|11\rangle)/N$ (N is the normalization coefficient). For the curve plotted with the full Hamiltonian, $\Delta = 20\Omega$ is used.

the effective Hamiltonian would be changed to

$$\hat{H}_{\text{eff}} = \frac{\Omega^2}{2\Delta}[(-|10\rangle + |11\rangle)\langle rr| + \text{H.c.}], \quad (23)$$

after choosing $\mu = 2$, based on which the standard controlled-NOT gate would be achieved at the time $t = \sqrt{2}\pi\Delta/\Omega^2$.

In Fig. 8, we use a specific initial state to estimate the performance of the gate. The numerical results show the consistency between the curves plotted by the full and effective Hamiltonian, respectively.

IV. IMPROVE THE PERFORMANCE OF THE DISSIPATIVE-DYNAMICS-BASED ENTANGLEMENT PREPARATION

In this section, we study the influence of the modified RAB regime on the dissipative-dynamics-based quantum entanglement preparation scheme.

A. Physical process

Considering the model shown in Fig. 9, the Hamiltonian of the whole system is $\hat{H} = \hat{H}_1 + \hat{H}_2$, where

$$\hat{H}_1 = \sum_{j=1,2} -\Delta|r\rangle_j\langle r| + \frac{\Omega}{2}(|r\rangle_j\langle 1| + |1\rangle_j\langle r|), \quad (24)$$

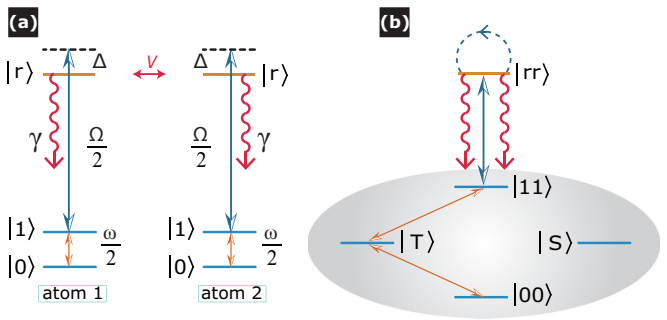

FIG. 9. (a) Energy diagram of the dissipative scheme to prepare steady entanglement. The coupling between $|1\rangle$ and $|r\rangle$ is dispersive with detuning $-\Delta$ and Rabi frequency Ω. And the transition between two ground states is driven by the resonant microwave field with Rabi frequency ω. The Rydberg state $|r\rangle$ decays to two ground states with a total spontaneous rate γ. (b) Diagram of the effective process of the dynamics under the two-atom basis.

and

$$\hat{H}_2 = \sum_{j=1,2} \frac{\omega}{2}(|1\rangle_j\langle 0| + |0\rangle_j\langle 1|). \quad (25)$$

Under the traditional RAB condition $V = 2\Delta$ and the dispersive regime, the effective form of Hamiltonian (24) can be written as

$$\hat{H}_1^{\text{eff}} = \frac{\Omega^2}{4\Delta}[2(|11\rangle + |rr\rangle)(\langle rr| + \langle 11|) + (|10\rangle\langle 10| + |01\rangle\langle 01|)]. \quad (26)$$

Under the two-atom basis, the microwave field Hamiltonian can be rewritten as

$$\hat{H}_2 = \frac{\sqrt{2}\omega}{2}[|00\rangle\langle T| + |T\rangle\langle 11| + \text{H.c.}], \quad (27)$$

in which $|T\rangle = (|01\rangle + |10\rangle)/\sqrt{2}$. The dark state of Hamiltonian (27) is $|S\rangle = (|01\rangle - |10\rangle)/\sqrt{2}$, which is the desired steady entanglement. Thus, one can get from Eq. (27) that the microwave field shuffles the states $|00\rangle$, $|T\rangle$, and $|11\rangle$, and keeps $|S\rangle$ invariant. The state $|11\rangle$ can be excited to $|rr\rangle$ via the effect of Hamiltonian (26) and further decayed to the ground-state subspace. Once $|S\rangle$ is populated, the scheme succeeds. Otherwise, if the other three states are populated, they would be re-excited and decay to the ground subspace again. The above processes get repeated until the scheme is successful.

B. Relationship between unitary dynamics and the dissipative process

Strictly speaking, the relationship between unitary dynamics and the dissipative process can be interpreted as unity of opposites between competition and cooperation, which makes the target state $|S\rangle$ the specific stationary state of the system. The unitary process $|11\rangle \to |rr\rangle$ is cooperative with the dissipative process, while the unitary processes $|rr\rangle \to |11\rangle$ and $|rr\rangle \to |rr\rangle$ are competitive with the dissipative process. One should be aware of the fact that, under the traditional RAB regime $\Delta = 2V$, the scheme is feasible [55,56]. The aim of introducing the modified RAB is to try to find a more optimal equilibrium point between competition and cooperation, which may improve the performance of the scheme. In Fig. 10, we use the master equation,

$$\dot{\hat{\rho}} = -i[\hat{H}, \hat{\rho}] + \frac{\gamma}{2}\sum_{j=1}^{4}(2\hat{\sigma}_j\hat{\rho}\hat{\sigma}_j^\dagger - \hat{\sigma}_j^\dagger\hat{\sigma}_j\hat{\rho} - \hat{\rho}\hat{\sigma}_j^\dagger\hat{\sigma}_j), \quad (28)$$

to solve numerically the dynamics of the system [67], where $\hat{\sigma}_1 = |0\rangle_1\langle r|$ and $\hat{\sigma}_2 = |1\rangle_1\langle r|$ denote the operators of atom 1, and $\hat{\sigma}_3 = |0\rangle_2\langle r|$, and $\hat{\sigma}_4 = |1\rangle_2\langle r|$ denote the operators of atom 2, respectively. In Fig. 10(a), we plot the fidelities versus μ to find the optimal value. In Fig. 10(b), we plot the fidelities versus evolution time under the traditional and modified RAB regimes with the optimal μ from Fig. 10(a). One can see that under the modified RAB regime the fidelity can be improved a little and the time to be steady is reduced.

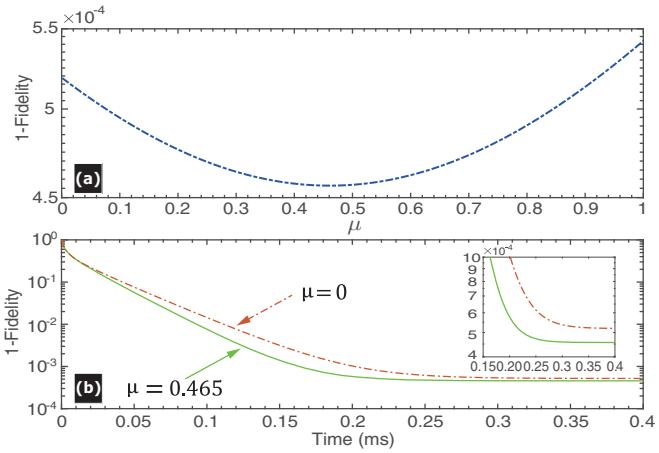

FIG. 10. (a) Fidelity of the steady entanglement versus μ under the modified RAB condition. (b) Fidelities of the entanglement versus evolution time with optimal $\mu = 0.465$ and $\mu = 0$ (traditional RAB regime). The parameters are chosen as $\Omega/2\pi = 0.036$ MHz, $\omega/2\pi = 1.45\times10^{-4}$ MHz, $\Delta = 3$ MHz, and $\gamma = 1.257$ KHz. The initial state is chosen as $|11\rangle$, and the target state is $|S\rangle$. For simplicity, we have assumed the Rydberg state has equal spontaneous rates on two ground states.

C. Differences of the unitary dynamics

We now aim to find some differences of the unitary dynamics process under the traditional and modified RAB regimes since the dissipative processes are almost the same as one another under these two regimes, and try to give some reasonable explanations why the performance is improved under the modified RAB regime. To do this we first write the effective Hamiltonian under the modified regime,

$$\hat{H}_1^{\text{eff}} = \frac{\Omega^2}{4\Delta}[2(|11\rangle\langle 11| + |rr\rangle\langle 11| + |11\rangle\langle rr|) + (2-2\mu)|rr\rangle\langle rr| + (|10\rangle\langle 10| + |01\rangle\langle 01|)]. \quad (29)$$

Then we use Eq. (29) to simulate the behaviors of the unitary dynamics, which is shown in Fig. 11. One can see that the amplitude of the Rabi oscillation under the modified RAB condition is slightly less than that under the traditional RAB regime. In other words, $|rr\rangle$ has not been converted to $|11\rangle$

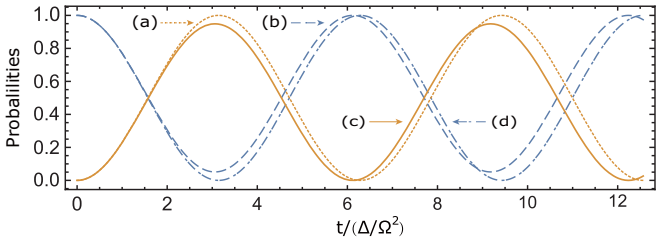

FIG. 11. (a) and (d) Probabilities of $|11\rangle$ ($|rr\rangle$) versus time under the traditional RAB regime. (b) and (c) Probabilities of $|rr\rangle$ ($|11\rangle$) versus time under the modified RAB regime with $\mu = 0.465$. We have set $|rr\rangle$ as the initial state. On the other hand, if $|11\rangle$ is considered as the initial state, the curve of the probability of $|rr\rangle$ is the same as (a) (traditional Rydberg antiblockade regime) or (c) (modified RAB regime).

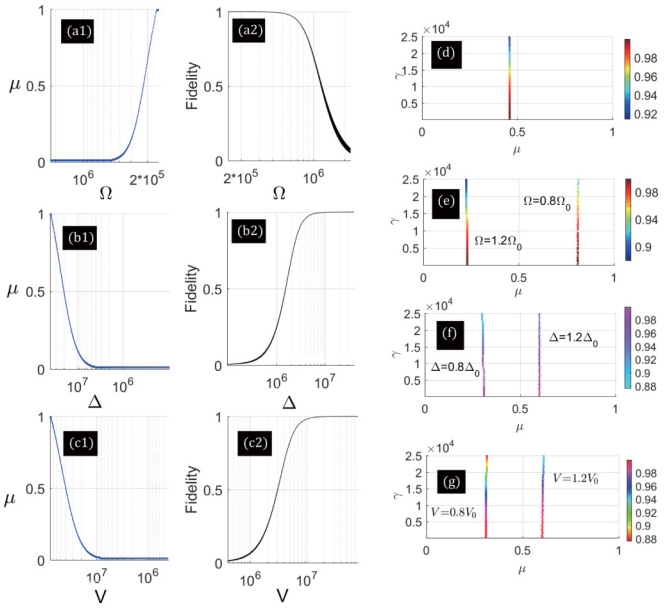

FIG. 12. (a1)–(c1) Optimal values of μ versus $\Omega(\Delta, V)$. (a2)–(c2)] Fidelity of the scheme versus $\Omega(\Delta, V)$ with μ being optimal. (d) Fidelity to reveal the optimal μ versus γ with parameters the same as that in Figs. 10. (e)–(g) Fidelity of the optimal μ versus γ, and the rest of the parameters are chosen the same as that in Fig. 10. For each $\Omega(\Delta, V, \gamma)$, we scan 200 groups of μ from 0 to 1 and find the top two fidelities. Ω_0 and Δ_0 are the same as Ω and Δ in Fig. 10, and $V_0 = 2\Delta_0$ are supposed.

completely in half period of Rabi oscillation. The role of the unitary process which is competitive with the dissipative process is decreased. And it was perhaps on this account that the whole performance of the scheme was enhanced a little. On the other hand, one can also find μ to further decrease the probabilities from $|rr\rangle$ to $|11\rangle$. Nevertheless, the probability of the process $|11\rangle \to |rr\rangle$, which is cooperative with the dissipative process, would also be decreased at the same time, and further reduce the whole performance of the scheme. Besides, the oscillation frequency of Figs. 11(b) and 11(c) is slightly faster than that of Figs. 11(a) and 11(d). That is, the speed of the energy exchange ($|11\rangle \leftrightarrow |rr\rangle$) of the modified RAB regime is slightly quicker than that of the traditional one. This may be the other reason for the improvement. The lowest point of Fig. 10(a) corresponding to the optimal balance point between the cooperative and competitive regimes.

D. Optimal μ for wide range of parameters

In practice, for a wide range of parameters Δ, Ω, V, and γ, it is necessary to discuss the optimal values of μ. In Figs. 12(a1)–12(c1), we plot the optimal values of μ versus $\Omega(\Delta, V)$, from which one can find the one-to-one relationship between $\Omega(\Delta, V)$ and μ. Besides, in Figs. 12(a2)–12(c2), we plot the fidelity of the scheme versus Ω with μ being optimal correspondingly. Since Ω and Δ can be optimized for a given V based on the RAB condition, one can always find the parameters to make the scheme optimal. However, this is not the case for the spontaneous emission rate γ which is not easily controlled. Fortunately, Figs. 12(d)–12(g) show that the optimal μ is almost independent of γ. From Fig. 12, it is easy to find that, with the optimal μ, the fidelity increases when Δ increases or Ω decreases. The reason is that the scheme works under the dispersive condition $\Delta \gg \Omega$.

V. DISCUSSIONS

A. Average fidelity with dissipation

The presented schemes are independent of the initial state in the strict scene, which motivates us to use the average fidelity to evaluate the performance of the logic gate. One of the common definitions of average fidelity for quantum logic gate is [68]

$$\overline{F} = \frac{1}{4\pi^2}\int_0^{2\pi} d\alpha \int_0^{2\pi} d\beta F(\alpha,\beta), \tag{30}$$

where the initial state is set as $(\cos\alpha|0\rangle_1 + \sin\alpha|1\rangle_1) \otimes (\cos\beta|0\rangle_2 + \sin\beta|1\rangle_2)$. And $F(\alpha,\beta) \equiv \mathrm{tr}\sqrt{\hat{\rho}^{1/2}(\alpha,\beta)\hat{\sigma}(\alpha,\beta)\hat{\rho}^{1/2}(\alpha,\beta)}$, in which $\hat{\sigma}(\alpha,\beta)$ is from the ideal quantum logic gate, and $\hat{\rho}(\alpha,\beta)$ is obtained from the practical logic gate. In Fig. 13, we plot the average fidelity of the quantum logic gate with approximate and accurate cases, respectively, versus γ with the full Hamiltonian. For the approximate quantum logic gates, the trend of the average fidelity versus γ are mainly affected by two factors. One is the length of the optimal evolution time (the longer evolution time would enhance the influences of the dissipation). The other is the perfectness of the optimal values from numerical simulations in Figs. 3 and 4. For instance, when $\mu = 2.25$, the transformation $|11\rangle \to 0.9979i|11\rangle$ is realized at the time $t = 8\pi\Delta/\Omega^2$. While for $\mu = 8$, $|11\rangle \to -0.9997i|11\rangle$ is realized with the same evolution time. Thus, the average fidelity of the latter case ($\mu = 7.75$) should be better than that of the former one ($\mu = 2.25$), which is consistent with the results in Fig. 13(a).

We use 1000 groups of pure states and mixed states as initial states, respectively, to test the performance of the modified RAB-regime-based state preparation scheme. As shown in

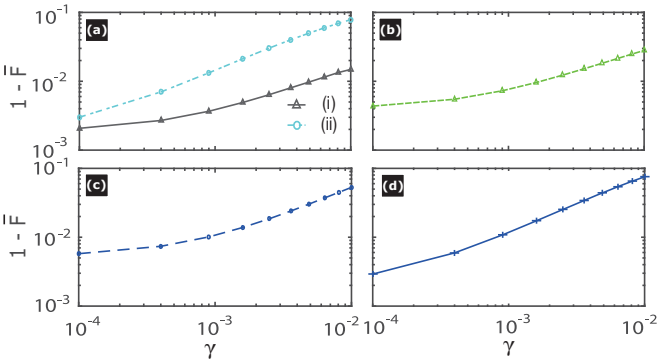

FIG. 13. (a) Average fidelity of the approximate controlled-PHASE gates versus γ at the time $8\pi\Delta/\Omega^2$: (i) $\mu = 7.75$, controlled-$-\frac{\pi}{2}$ gate; (ii) $\mu = 2.25$, controlled-$\frac{\pi}{2}$ gate. (b) Average fidelity of the approximate controlled-NOT′ gate versus γ with $\mu = 7.5$ at the time $8\pi\Delta/\Omega^2$. (c) Average fidelity of the accurate controlled-NOT gate versus γ with $\mu = 2$ at the optimal time $t = \sqrt{2}\pi\Delta/\Omega^2$. (d) Average fidelity of the accurate controlled-π gate. $\Delta = 10\Omega$ is assumed for the above simulations.

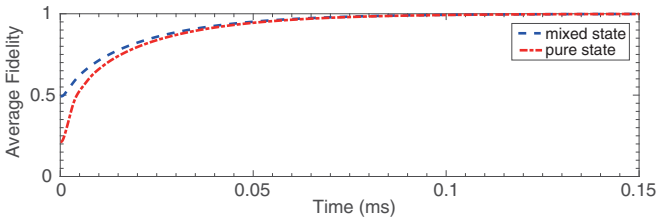

FIG. 14. Average fidelity of the modified RAB-regime-based scheme with 1000 groups of the initially mixed state and pure state, respectively. The parameters are the same as those used in Fig. 10(b).

Fig. 14, one can find that the $|S\rangle$ state can be prepared with high fidelity for these two cases.

B. Influence of the parameter fluctuations

In practical situations, the parameters would no doubt fluctuate and influence the performance of the scheme. One of the main considerations is the fluctuation of V induced by atomic motion. Without loss of generality, we suppose the fluctuation of V satisfying the Gauss distribution with mean V_0 and standard deviation δV. In Fig. 15, we use the full Hamiltonian to simulate numerically the evolution process. For a fixed δV, the mean value of the fidelity is calculated as $F_A = (\sum_{j=1}^{j=m} \overline{F}^j_{\max})/m$, in which $\overline{F}^j_{\max}$ is obtained from Eq. (30). The results show the schemes corresponding to Figs. 15(a) and 15(b) have better robustness on the fluctuation of V than those corresponding to Figs. 15(c) and 15(d). For the schemes corresponding to Figs. 15(a) and 15(b), there may exist many values of V satisfying the scheme approximately, which may induce the good robustness. Nevertheless, the RAB condition of the schemes corresponding to Figs. 15(c) and 15(d) are unique. Besides, in Fig. 16, we plot the influences

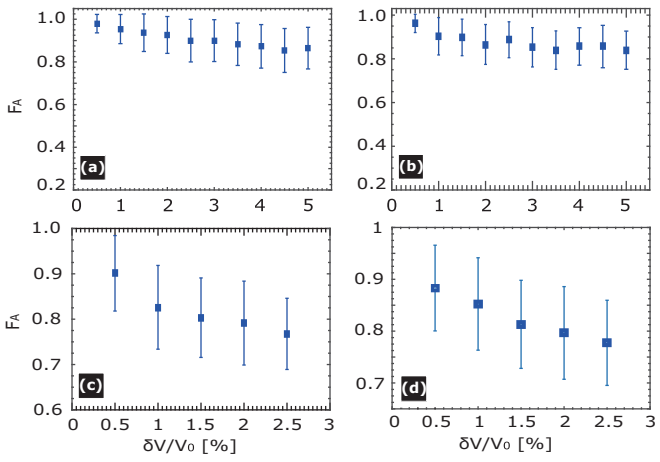

FIG. 15. Average fidelity of the modified RAB-regime-based quantum logic gates versus scaled standard deviations of inhomogeneous parameters V with $m = 100$ at the optimal evolution time. (a) The approximate controlled-$-\frac{\pi}{2}$ gate. (b) and (c) The controlled-NOT gate with the schematic in Figs. 6(a) and 6(b). (d) The accurate controlled-π gate. Parameters are chosen as $\Delta = 10\Omega, \gamma = 10^{-4}\Omega$, (a) $\mu = 7.75$, (b) $\mu = 7.5$, (c) $\mu = 2$, and (d) $\mu = \sqrt{4/3}$.

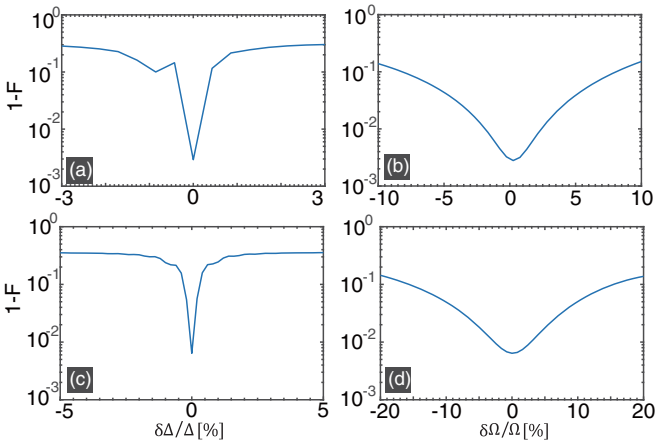

FIG. 16. (a) and (b) Fidelities of the accurate controlled-PHASE gate (without loss of generality, we here consider $\theta = \pi$) versus the deviation of Δ (Ω) under Eq. (30). (c) and (d) Fidelities of the accurate controlled-NOT gate versus deviation of Δ (Ω) with the initial state $|\psi_0\rangle = (0.1|00\rangle + 0.1|01\rangle + 0.4|10\rangle + 0.1|11\rangle)/N$ (N is the normalization coefficient). $\Delta = 10\Omega$ and $\gamma = 10^{-4}\Omega$ are used.

of the fluctuation of Ω and Δ on the accurate quantum controlled-π and controlled-NOT gates, respectively. One can see that the fluctuation of Δ has more influences than that of Ω. The reason is that Δ is greater than Ω and thus the RAB condition Eq. (5) is sensitive on the fluctuation of Δ.

VI. CONCLUSION

In conclusion, we modify the traditional simultaneous-driving-based RAB regime through the effective dynamics obtained from the second-order perturbation theory. In contrast to the traditional simultaneous-driving-based antiblockade regime, the modified one enriches the dynamics process and applications in QIP, including approximate and accurate quantum logic gates and dissipation-assisted quantum entanglement without adding any additional controls and resources. Thus, the experimental complexity of the scheme is not increased when the applications of the RAB with simultaneous driving is improved and enriched. In the future, generalizing the present modified RAB regime to Rydberg dressing atoms [31–39] is one of our study goals.

ACKNOWLEDGMENTS

This work was supported by China Postdoctoral Science Foundation under Grant No. 2017M612411; Subject Construction Project of School of Physics of Northeast Normal University under Grant No. 111715014; China Postdoctoral Science Foundation under Grants No. 2016M600223 and No. 2017T100192; Fundamental Research Funds for the Central Universities under Grant No. 2412017QD005; National Natural Science Foundation of China under Grants No. 11705025, No. 61465013, and No. 11404290; and Natural Science Foundation of Henan Educational Committee (Grant No. 17A140002).

APPENDIX: DERIVATION OF EQ. (6)

The full Hamiltonian in the interaction picture can be written as

$$\hat{H} = \frac{\Omega}{2}[(|r\rangle_1\langle 1| + |r\rangle_2\langle 1|)e^{-i\Delta t} + \text{H.c.}] + V|rr\rangle\langle rr|, \quad \text{(A1)}$$

which can be transformed to

$$\hat{H} = \frac{\Omega}{2}[e^{i\Delta t}(|01\rangle\langle 0r| + |11\rangle\langle 1r| + |10\rangle\langle r0| + |11\rangle\langle r1| + |r1\rangle\langle rr| + |1r\rangle\langle rr|) + \text{H.c.}] + V|rr\rangle\langle rr|, \quad \text{(A2)}$$

under the two-atom basis. After considering the modified RAB condition in Eq. (5) and moving Hamiltonian (A2) to the rotation frame with respect to $\hat{U}_0^\dagger \equiv e^{i\hat{H}_0 t}$ with $\hat{H}_0 = 2\Delta|rr\rangle\langle rr|$, one can get

$$\hat{H}' = \frac{\Omega}{2}[e^{i\Delta t}(|01\rangle\langle 0r| + |11\rangle\langle 1r| + |10\rangle\langle r0| + |11\rangle\langle r1| + |rr\rangle\langle r1| + |rr\rangle\langle 1r|) + \text{H.c.}] - \mu\frac{\Omega^2}{2\Delta}|rr\rangle\langle rr|, \quad \text{(A3)}$$

in which the formula $\hat{H}' = -\hat{H}_0 + \hat{U}_0^\dagger \hat{H} \hat{U}_0$ is used. Under the large detuning regime $\Delta \gg \Omega/2$, one can get the effective Hamiltonian as [61]

$$\hat{H}'_{\text{eff}} = \frac{\Omega^2}{2\Delta}(|11\rangle + |rr\rangle)(\langle rr| + \langle 11|) + \frac{\Omega^2}{4\Delta}(|10\rangle\langle 10| + |01\rangle\langle 01|) - \mu\frac{\Omega^2}{2\Delta}|rr\rangle\langle rr|, \quad \text{(A4)}$$

which is the same as Eq. (6). Two things are worth mentioning about this effective Hamiltonian. (i) We have discarded the terms in single excitation subspace since they are not included in the initial states and do not exchange energy with the states in the other subspace. (ii) Strictly speaking, the dynamics of the whole system is governed by $e^{-iH_0 t}e^{-iH'_{\text{eff}}t}$ [69]. However, our scheme requires that under the control of the evolution operator $e^{-iH'_{\text{eff}}t}$, the amplitude of $|rr\rangle$ should be zero approximately at the optimal evolution time since $|rr\rangle$ is out of the computational subspace. In this case, the $e^{-iH_0 t}$ has no influence and we thus do not consider it.

[1] D. Jaksch, J. I. Cirac, P. Zoller, S. L. Rolston, R. Côté, and M. D. Lukin, Fast Quantum Gates for Neutral Atoms, Phys. Rev. Lett. **85**, 2208 (2000).

[2] M. D. Lukin, M. Fleischhauer, R. Côté, L. M. Duan, D. Jaksch, J. I. Cirac, and P. Zoller, Dipole Blockade and Quantum Information Processing in Mesoscopic Atomic Ensembles, Phys. Rev. Lett. **87**, 037901 (2001).

[3] T. F. Gallagher, *Rydberg Atoms* (Cambridge University Press, Cambridge, 1994).

[4] M. Saffman, T. G. Walker, and K. Mølmer, Quantum information with Rydberg atoms, Rev. Mod. Phys. **82**, 2313 (2010).

[5] M. Saffman, Quantum computing with atomic qubits and Rydberg interactions: progress and challenges, J. Phys. B **49**, 202001 (2016).

[6] E. Brion, A. S. Mouritzen, and K. Mølmer, Conditional dynamics induced by new configurations for Rydberg dipole-dipole interactions, Phys. Rev. A **76**, 022334 (2007).

[7] M. Müller, I. Lesanovsky, H. Weimer, H. P. Büchler, and P. Zoller, Mesoscopic Rydberg Gate Based on Electromagnetically Induced Transparency, Phys. Rev. Lett. **102**, 170502 (2009).

[8] H. Z. Wu, Z. B. Yang, and S. B. Zheng, Implementation of a multiqubit quantum phase gate in a neutral atomic ensemble via the asymmetric Rydberg blockade, Phys. Rev. A **82**, 034307 (2010).

[9] L. Isenhower, M. Saffman, and K. Mølmer, Multibit C_kNOT quantum gates via Rydberg blockade, Quantum Inf. Process. **10**, 755 (2011).

[10] M. Saffman and K. Mølmer, Efficient Multiparticle Entanglement via Asymmetric Rydberg Blockade, Phys. Rev. Lett. **102**, 240502 (2009).

[11] D. Møller, L. B. Madsen, and K. Mølmer, Quantum Gates and Multiparticle Entanglement by Rydberg Blockade and Adiabatic Passage, Phys. Rev. Lett. **100**, 170504 (2008).

[12] I. I. Beterov, M. Saffman, E. A. Yakshina, V. P. Zhukov, D. B. Tretyakov, V. M. Entin, I. I. Ryabtsev, C. W. Mansell, C. MacCormick, S. Bergamini, and M. P. Fedoruk, Quantum gates in mesoscopic atomic ensembles based on adiabatic passage and Rydberg blockade, Phys. Rev. A **88**, 010303(R) (2013).

[13] M. M. Müller, M. Murphy, S. Montangero, T. Calarco, P. Grangier, and A. Browaeys, Implementation of an experimentally feasible controlled-phase gate on two blockaded Rydberg atoms, Phys. Rev. A **89**, 032334 (2014).

[14] D. Petrosyan and K. Mølmer, Binding Potentials and Interaction Gates Between Microwave-Dressed Rydberg Atoms, Phys. Rev. Lett. **113**, 123003 (2014).

[15] D. D. Bhaktavatsala Rao and K. Mølmer, Robust Rydberg-interaction gates with adiabatic passage, Phys. Rev. A **89**, 030301(R) (2014).

[16] X. D. Tian, Y. M. Liu, C. L. Cui, and J. H. Wu, Population transfer and quantum entanglement implemented in cold atoms involving two Rydberg states via an adiabatic passage, Phys. Rev. A **92**, 063411 (2015).

[17] I. I. Beterov, M. Saffman, E. A. Yakshina, D. B. Tretyakov, V. M. Entin, S. Bergamini, E. A. Kuznetsova, and I. I. Ryabtsev, Two-qubit gates using adiabatic passage of the Stark-tuned Förster resonances in Rydberg atoms, Phys. Rev. A **94**, 062307 (2016).

[18] L. S. Theis, F. Motzoi, F. K. Wilhelm, and M. Saffman, High-fidelity Rydberg-blockade entangling gate using shaped, analytic pulses, Phys. Rev. A **94**, 032306 (2016).

[19] D. Tong, S. M. Farooqi, J. Stanojevic, S. Krishnan, Y. P. Zhang, R. Côté, E. E. Eyler, and P. L. Gould, Local Blockade of Rydberg Excitation in an Ultracold Gas, Phys. Rev. Lett. **93**, 063001 (2004).

[20] K. Singer, M. Reetz-Lamour, T. Amthor, L. G. Marcassa, and M. Weidemüller, Suppression of Excitation and Spectral Broadening Induced by Interactions in a Cold Gas of Rydberg Atoms, Phys. Rev. Lett. **93**, 163001 (2004).

[21] T. C. Liebisch, A. Reinhard, P. R. Berman, and G. Raithel, Atom Counting Statistics in Ensembles of Interacting Rydberg Atoms, Phys. Rev. Lett. **95**, 253002 (2005).

[22] R. Heidemann, U. Raitzsch, V. Bendkowsky, B. Butscher, R. Löw, L. Santos, and T. Pfau, Evidence for Coherent Collective

Rydberg Excitation in the Strong Blockade Regime, Phys. Rev. Lett. **99**, 163601 (2007).
[23] E. Urban, T. A. Johnson, T. Henage, L. Isenhower, D. D. Yavuz, T. G. Walker, and M. Saffman, Observation of Rydberg blockade between two atoms, Nat. Phys. **5**, 110 (2009).
[24] A. Gaëtan, Y. Miroshnychenko, T. Wilk, A. Chotia, M. Viteau, D. Comparat, P. Pillet, A. Browaeys, and P. Grangier, Observation of collective excitation of two individual atoms in the Rydberg blockade regime, Nat. Phys. **5**, 115 (2009).
[25] T. Wilk, A. Gaëtan, C. Evellin, J. Wolters, Y. Miroshnychenko, P. Grangier, and A. Browaeys, Entanglement of Two Individual Neutral Atoms Using Rydberg Blockade, Phys. Rev. Lett. **104**, 010502 (2010).
[26] J. D. Pritchard, D. Maxwell, A. Gauguet, K. J. Weatherill, M. P. A. Jones, and C. S. Adams, Cooperative Atom-Light Interaction in a Blockaded Rydberg Ensemble, Phys. Rev. Lett. **105**, 193603 (2010).
[27] Y. O. Dudin and A. Kuzmich, Strongly interacting Rydberg excitations of a cold atomic gas, Science **336**, 887 (2012).
[28] Y. O. Dudin, L. Li, F. Bariani, and A. Kuzmich, Observation of coherent many-body Rabi oscillations, Nat. Phys. **8**, 790 (2012).
[29] P. Schauß, M. Cheneau, M. Endres, T. Fukuhara, S. Hild, A. Omran, T. Pohl, C. Gross, S. Kuhr, and I. Bloch, Observation of spatially ordered structures in a two-dimensional Rydberg gas, Nature (London) **491**, 87 (2012).
[30] G. Günter, H. Schempp, M. Robert-de-Saint-Vincent, V. Gavryusev, S. Helmrich, C. S. Hofmann, S. Whitlock, and M. Weidemuller, Observing the dynamics of dipole-mediated energy transport by interaction-enhanced imaging, Science **342**, 954 (2013).
[31] L. Santos, G. V. Shlyapnikov, P. Zoller, and M. Lewenstein, Bose-Einstein Condensation in Trapped Dipolar Gases, Phys. Rev. Lett. **85**, 1791 (2000).
[32] J. E. Johnson and S. L. Rolston, Interactions between Rydberg-dressed atoms, Phys. Rev. A **82**, 033412 (2010).
[33] T. Keating, K. Goyal, Y. Y. Jau, G. W. Biedermann, A. J. Landahl, and I. H. Deutsch, Adiabatic quantum computation with Rydberg-dressed atoms, Phys. Rev. A **87**, 052314 (2013).
[34] J. B. Balewski, A. T. Krupp, A. Gaj, S. Hofferberth, R. Löw, and T. Pfau, Rydberg dressing: Understanding of collective many-body effects and implications for experiments, New J. Phys. **16**, 063012 (2014).
[35] T. Macrì and T. Pohl, Rydberg dressing of atoms in optical lattices, Phys. Rev. A **89**, 011402(R) (2014).
[36] T. Keating, R. L. Cook, A. M. Hankin, Y. Y. Jau, G. W. Biedermann, and I. H. Deutsch, Robust quantum logic in neutral atoms via adiabatic Rydberg dressing, Phys. Rev. A **91**, 012337 (2015).
[37] L. F. Buchmann, K. Mølmer, and D. Petrosyan, Creation and transfer of nonclassical states of motion using Rydberg dressing of atoms in a lattice, Phys. Rev. A **95**, 013403 (2017).
[38] M. Płodzień, G. Lochead, J. de Hond, N. J. van Druten, and S. Kokkelmans, Rydberg dressing of a one-dimensional Bose-Einstein condensate, Phys. Rev. A **95**, 043606 (2017).
[39] J. M. Lee, M. J. Martin, Y. Y. Jau, T. Keating, I. H. Deutsch, and G. W. Biedermann, Demonstration of the Jaynes-Cummings ladder with Rydberg-dressed atoms, Phys. Rev. A **95**, 041801(R) (2017).
[40] J. Zeiher, R. van Bijnen, P. Schauß, S. Hild, J. Y. Choi, T. Pohl, I. Bloch, and C. Gross, Many-body interferometry of a Rydberg-dressed spin lattice, Nat. Phys. **12**, 1095 (2016).
[41] Y. Y. Jau, A. M. Hankin, T. Keating, I. H. Deutsch, and G. W. Biedermann, Entangling atomic spins with a Rydberg-dressed spin-flip blockade, Nat. Phys. **12**, 71 (2016).
[42] S. Baur, D. Tiarks, G. Rempe, and S. Dürr, Single-Photon Switch Based on Rydberg Blockade, Phys. Rev. Lett. **112**, 073901 (2014).
[43] D. Petrosyan, D. D. B. Rao, and K. Mølmer, Filtering single atoms from Rydberg-blockaded mesoscopic ensembles, Phys. Rev. A **91**, 043402 (2015).
[44] H. Gorniaczyk, C. Tresp, J. Schmidt, H. Fedder, and S. Hofferberth, Single-Photon Transistor Mediated by Interstate Rydberg Interactions, Phys. Rev. Lett. **113**, 053601 (2014).
[45] D. Tiarks, S. Baur, K. Schneider, S. Dürr, and G. Rempe, Single-Photon Transistor Using a Forster Resonance, Phys. Rev. Lett. **113**, 053602 (2014).
[46] A. V. Gorshkov, J. Otterbach, M. Fleischhauer, T. Pohl, and M. D. Lukin, Photon-Photon Interactions via Rydberg Blockade, Phys. Rev. Lett. **107**, 133602 (2011).
[47] S. Das, A. Grankin, I. Iakoupov, E. Brion, J. Borregaard, R. Boddeda, I. Usmani, A. Ourjoumtsev, P. Grangier, and A. S. Sørensen, Photonic controlled-phase gates through Rydberg blockade in optical cavities, Phys. Rev. A **93**, 040303(R) (2016).
[48] H. Z. Shen, Y. H. Zhou, and X. X. Yi, Quantum optical diode with semiconductor microcavities, Phys. Rev. A **90**, 023849 (2014); Tunable photon blockade in coupled semiconductor cavities, **91**, 063808 (2015).
[49] C. Ates, T. Pohl, T. Pattard, and J. M. Rost, Antiblockade in Rydberg Excitation of an Ultracold Lattice Gas, Phys. Rev. Lett. **98**, 023002 (2007).
[50] T. Amthor, C. Giese, C. S. Hofmann, and M. Weidemüller, Evidence of Anti-Blockade in an Ultracold Rydberg Gas, Phys. Rev. Lett. **104**, 013001 (2010).
[51] T. Pohl and P. R. Berman, Breaking the Dipole Blockade: Nearly Resonant Dipole Interactions in Few-Atom Systems, Phys. Rev. Lett. **102**, 013004 (2009).
[52] J. Qian, Y. Qian, M. Ke, X. L. Feng, C. H. Oh, and Y. Z. Wang, Breakdown of the dipole blockade with a zero-area phase-jump pulse, Phys. Rev. A **80**, 053413 (2009).
[53] Z. C. Zuo and K. Nakagawa, Multiparticle entanglement in a one-dimensional optical lattice using Rydberg-atom interactions, Phys. Rev. A **82**, 062328 (2010).
[54] T. E. Lee, H. Häffner, and M. C. Cross, Collective Quantum Jumps of Rydberg Atoms, Phys. Rev. Lett. **108**, 023602 (2012).
[55] A. W. Carr and M. Saffman, Preparation of Entangled and Antiferromagnetic States by Dissipative Rydberg Pumping, Phys. Rev. Lett. **111**, 033607 (2013).
[56] S. L. Su, Q. Guo, H. F. Wang, and S. Zhang, Simplified scheme for entanglement preparation with Rydberg pumping via dissipation, Phys. Rev. A **92**, 022328 (2015).
[57] S. L. Su, Y. Gao, E. J. Liang, and S. Zhang, Fast Rydberg antiblockade regime and its applications in quantum logic gates, Phys. Rev. A **95**, 022319 (2017).
[58] A. M. Hankin, Y.-Y. Jau, L. P. Parazzoli, C. W. Chou, D. J. Armstrong, A. J. Landahl, and G. W. Biedermann, Two-atom Rydberg blockade using direct 6*S* to *nP* excitation, Phys. Rev. A **89**, 033416 (2014).

[59] W. Li, C. Ates, and I. Lesanovsky, Nonadiabatic Motional Effects and Dissipative Blockade for Rydberg Atoms Excited From Optical Lattices or Microtraps, Phys. Rev. Lett. **110**, 213005 (2013).

[60] X. Q. Shao, J. H. Wu, and X. X. Yi, Dissipation-based entanglement via quantum Zeno dynamics and Rydberg antiblockade, Phys. Rev. A **95**, 062339 (2017).

[61] D. F. V. James and J. Jerke, Effective Hamiltonian theory and its applications in quantum information, Can. J. Phys. **85**, 625 (2007).

[62] If the initial state is $|11\rangle$, the state at time t would be $[(1+e^{-i\Omega^2 t/\Delta})|11\rangle+(-1+e^{-i\Omega^2 t/\Delta})|rr\rangle]/2$. Since $|rr\rangle$ is out of the computation subspace $\{|00\rangle,|01\rangle,|10\rangle,|11\rangle\}$, the coefficient of it should be zero and thus the transformation $|11\rangle\rightarrow|11\rangle$ is realized, which implies that the quantum controlled-PHASE gate cannot be constructed in one step.

[63] The distance between optically trapped Rydberg atoms are always considered invariant, which induces the distance-dependent Rydberg-Rydberg interaction V being constant ideally. Thus, to achieve the modified RAB condition, one should adjust the rest parameters Δ or Ω or both of them. $\Delta=\frac{1}{4}(V+\sqrt{V^2+4\mu\Omega^2})$ or $\Omega=\pm\sqrt{\frac{4\Delta^2-2\Delta V}{\mu}}$ can make Eq. (5) true. Currently, Δ and Ω are relatively easy to control and adjust, which means the realization of the modified RAB regime is not harder than the traditional one.

[64] C. Y. Chen, M. Feng, and K. L. Gao, Toffoli gate originating from a single resonant interaction with cavity QED, Phys. Rev. A **73**, 064304 (2006).

[65] In fact, there will be more choices for μ at the time $t=24\pi\Delta/\Omega^2$ to construct the quantum logic gate. However, the influence of the decoherence enhances as the evolution time increases. Therefore, we do not consider the case $t=24\pi\Delta/\Omega^2$ and other cases with much longer evolution time.

[66] M. A. Nielsen and I. L. Chuang, *Quantum Computation and Quantum Information* (Cambridge University Press, Cambridge, 2000).

[67] S. M. Tan, A computational toolbox for quantum and atomic optics, J. Opt. B: Quantum Semiclass. Opt. **1**, 424 (1999).

[68] Z. Q. Yin and F. L. Li, Multiatom and resonant interaction scheme for quantum state transfer and logical gates between two remote cavities via an optical fiber, Phys. Rev. A **75**, 012324 (2007).

[69] S.-B. Zheng, Generation of entangled states for many multilevel atoms in a thermal cavity and ions in thermal motion, Phys. Rev. A **68**, 035801 (2003).